

Nonreciprocal interactions induce frequency shifts in superradiant lasers

Tobias Nadolny,¹ Matteo Brunelli,² and Christoph Bruder¹

¹*Department of Physics, University of Basel, Klingelbergstrasse 82, 4056 Basel, Switzerland*

²*JEIP, UAR 3573 CNRS, Collège de France, PSL Research University,
11 Place Marcelin Berthelot, 75321 Paris Cedex 05, France*

(Dated: January 23, 2025)

Superradiant lasers, which consist of incoherently driven atoms coupled to a lossy cavity, are a promising source of coherent light due to their stable frequency and superior narrow linewidth. We show that when a fraction of the atoms is not driven, a shift in the lasing frequency and a broadening of the linewidth occur, limiting the performance of a superradiant laser. We explain this behavior by identifying nonreciprocal interactions between driven and undriven atoms, i.e., competing alignment and antialignment of their dipoles. Our results have implications for the realization of superradiant lasers, establishing the relevance of nonreciprocal phenomena for quantum technologies.

Superradiant lasers harness the coherence of a large ensemble of atoms that are collectively coupled to a cavity mode to provide light with narrow linewidth [1–3]. In contrast to a standard laser, the cavity decays rapidly ensuring a small number of excitations in the cavity mode, which renders the laser robust against cavity fluctuations [4, 5]. The laser light exhibits a stable frequency set by the atomic transition frequency. Continuous lasing can be achieved by incoherently driving each atom to provide it with energy [5–7]. Superradiant lasers offer great technological promise as their exceptionally narrow linewidth is expected to significantly improve the precision of optical atomic clocks [8].

In this letter, we study a superradiant laser where a fraction of the atoms is *not* driven; see Figs. 1(a,b). Surprisingly, this modification results in a shift of the lasing frequency and spectral broadening, which may be detrimental to the superradiant laser being used as a stable frequency reference with narrow linewidth. This contrasts with the expectation that the undriven atoms behave as passive spectators, causing only a reduction of the laser power. To explain this result, we show that driven and undriven atoms interact in a nonreciprocal way.

Nonreciprocal interactions mean that entities influence each other in asymmetric ways. They are an exciting feature of active matter [9, 10], i.e., an ensemble of interacting active agents, resulting in nonreciprocal phase transitions [11–13] and emergent time-crystalline order [14]. Here, we consider the superradiant laser as quantum active matter and the atomic dipoles as quantum active agents that can interact in a nonreciprocal way. We find that the driven atoms tend to align their dipole with the dipoles of both driven and undriven atoms; the undriven atoms, however, have the opposite inclination: they tend to align their dipoles opposite to those of all other atoms; see Figs. 1(c-e). The competition of alignment and antialignment results in chase-and-run-away dynamics of the atomic dipoles, which translates to a frequency shift

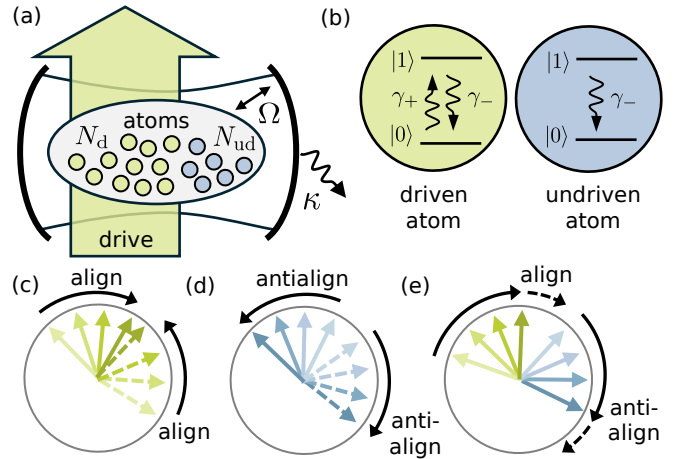


FIG. 1. (a) Superradiant laser, where N_d atoms are driven and $N_{ud} = N - N_d$ are undriven. All atoms are coupled at rate Ω to the cavity which decays at rate κ . (b) Incoherent gain and loss processes within each atomic spin. (c) Alignment between two driven atomic dipoles (solid and dashed straight arrows). Light to darker color indicates increasing time. (d) Antialignment between two undriven dipoles. (e) Nonreciprocal interactions between driven and undriven dipoles. The dashed circular arrows indicate the continuous motion.

of the laser. The antialignment itself decreases the coherence among the atoms, causing spectral broadening and loss of power.

Our work connects fundamental concepts of active matter with quantum technologies by showing that nonreciprocal interactions have practical implications for the development of superradiant lasers. Furthermore, our model offers a physical realization of conformist-contrarian dynamics, introduced in Refs. [15, 16] inspired by social behavior, whose implementation remained unclear. More broadly, our findings contribute to the understanding of nonreciprocal phenomena in quantum systems. Recent studies have shown that nonreciprocal interactions can be engineered by carefully designed light-

matter couplings [17–19]. The present work demonstrates that quantum nonreciprocal interactions can naturally occur between driven and undriven constituents.

Model.—We describe a superradiant laser, which comprises N atoms each modeled as a quantum spin-1/2 with states $|0\rangle$ and $|1\rangle$; see Fig. 1. While all spins are coupled coherently to a lossy cavity mode, only $N_d \leq N$ of the spins are incoherently driven; the other $N_{ud} = N - N_d$ spins are not driven. The fraction of driven (undriven) spins is $p_d = N_d/N$ ($p_{ud} = 1 - p_d$). The spins are described by Pauli matrices $\sigma_{\mu,i}^z = |1\rangle\langle 1|_{\mu,i} - |0\rangle\langle 0|_{\mu,i}$ and ladder operators $\sigma_{\mu,i}^+ = |1\rangle\langle 0|_{\mu,i}$, $\sigma_{\mu,i}^- = |0\rangle\langle 1|_{\mu,i}$. The index $\mu \in \{d, ud\}$ distinguishes driven and undriven spins, and i ranges from 1 to N_μ . The collective spin operators are $S^\pm = \sum_{i=1}^{N_d} \sigma_{d,i}^\pm + \sum_{i=1}^{N_{ud}} \sigma_{ud,i}^\pm$.

The quantum Lindblad master equation for the density operator ρ is

$$\dot{\rho} = -i\Omega[a^\dagger S^- + a S^+, \rho] + \kappa \mathcal{D}[a]\rho + \gamma_+ \sum_{i=1}^{N_d} \mathcal{D}[\sigma_{d,i}^+]\rho, \quad (1)$$

where $\mathcal{D}[o]\rho = o\rho o^\dagger - (o^\dagger o \rho + \rho o^\dagger o)/2$ is the Lindblad dissipator. Both the atomic spins and the cavity are described in the frame rotating with their bare frequencies, which are set equal. All spins couple equally with strength Ω to the cavity mode a , which decays at a rate κ . The last term in Eq. (1) describes an incoherent drive at rate γ_+ , which can be engineered by driving the state $|0\rangle$ to a third state which rapidly decays to state $|1\rangle$. For the case of all atoms being driven, $N_d = N$, the master equation reduces to the model studied in Ref. [3].

Emission spectrum.—A key quantity to characterize a laser is the spectral density $S(t, \omega)$ of light emitted by the cavity per frequency ω ,

$$S(t, \omega) = \int_{-\infty}^{\infty} d\tau \langle a^\dagger(t + \tau) a(t) \rangle e^{i\omega\tau}. \quad (2)$$

The steady-state spectrum is defined as $S(\omega) = \lim_{t \rightarrow \infty} S(t, \omega)$. The spectrum of a high-quality laser comprises a large and narrow peak, implying large output power and small linewidth. The spectrum can be calculated by employing a cumulant expansion approximation and the quantum regression theorem [3, 20–24]. The approximation amounts to neglecting third and higher-order correlations.

Figures 2(a,b) show the steady-state spectrum for the model defined in Eq. (1) as a function of p_d . If all spins are driven, $p_d = 1$, they collectively emit photons in a superradiant way into the cavity mode, which outputs highly coherent light as indicated by the narrow peak in the spectrum at zero frequency (in the frame rotating with the atomic frequency); When decreasing p_d , there are two peaks in the spectrum at nonzero frequencies indicating a positive or negative shift in the lasing frequency. Furthermore, for p_d smaller than a critical value, the peaks vanish indicating the absence of lasing.

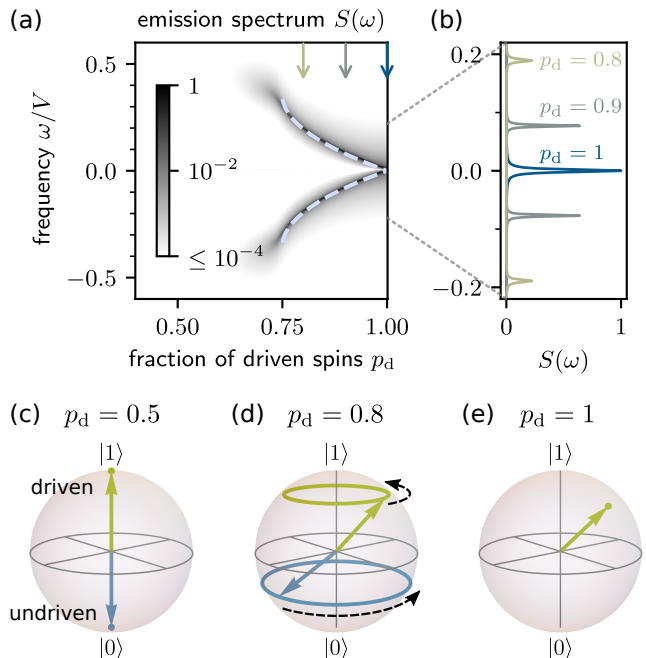


FIG. 2. (a) Cavity emission spectrum $S(\omega)$ (arb. units) as a function of fraction $p_d = N_d/N$ of driven spins for $N = 10^3$, $\kappa = 10\sqrt{N}\Omega$, and $V = \gamma_+$. The dashed line indicates the mean-field frequency. Below the lasing transition $p_d < 3/4$ [see Eq. (6)], the emission is close to zero. (b) Line cuts through (a) as marked by the three arrows in (a) on a linear scale. (c-e) Solutions of the mean-field equations (3) in the long-time limit displayed on the Bloch sphere for (c) $p_d = 0.5$: no lasing, (d) $p_d = 0.8$: lasing with frequency shift, and (e) $p_d = 1$: standard superradiant laser. The arrows indicate the state in the long-time limit. In (e), the dashed curved arrows indicate the continuous oscillations.

Nonreciprocal interactions.—We now explain the origin of the frequency shift displayed in Figs. 2(a,b). First, we derive an effective spin-only description. In the bad-cavity limit where $\kappa/(\sqrt{N}\Omega)$ is large, the cavity field instantaneously follows the spins, $a = -i(2\Omega/\kappa)S^-$, and can be adiabatically eliminated. Next, we exploit the permutational invariance: All driven spins are identical to one another and all undriven spins are identical to one another. In the thermodynamic limit, $N \rightarrow \infty$, Eq. (1) can thus be solved exactly using a mean-field ansatz [25, 26]. Introducing the coherences $s_\mu^+ = \langle \sigma_{\mu,i}^+ \rangle$, populations $s_\mu^z = \langle \sigma_{\mu,i}^z \rangle$, and the average coherence $s^+ = p_d s_d^+ + p_{ud} s_{ud}^+$, the mean-field equations are

$$\begin{aligned} \dot{s}_d^+ &= V s^+ s_d^z - \gamma_+ s_d^+ / 2, \\ \dot{s}_d^z &= -4V \text{Re}[s_d^- s^+] + \gamma_+ (1 - s_d^z), \\ \dot{s}_{ud}^+ &= V s^+ s_{ud}^z, \quad \dot{s}_{ud}^z = -4V \text{Re}[s_{ud}^- s^+]. \end{aligned} \quad (3)$$

Here, $V = 2N\Omega^2/\kappa$ is the effective dissipative coupling strength among all spins. Since we have not yet included any decay or dephasing of the spins, the purity of the

undriven spins is conserved, $(s_{\text{ud}}^z)^2 + 4s_{\text{ud}}^+ s_{\text{ud}}^- = \text{const} \leq 1$.

Equations (3) imply that the coherence of driven (undriven) spins tends to align in (out of) phase with respect to the average coherence. This becomes explicit in the dynamical equations for the phases $\phi_\mu = \arg(s_\mu^+)$ and the average phase $\bar{\phi} = \arg(s^+)$ derived from Eq. (3)

$$\dot{\phi}_\mu = s_\mu^z \frac{V|s^+|}{|s_\mu^+|} \sin(\bar{\phi} - \phi_\mu). \quad (4)$$

The sign of the term multiplying the sine determines whether ϕ_μ aligns or antialigns with $\bar{\phi}$. In a standard superradiant laser, all spins are driven, and their population is inverted $s_{\text{d}}^z > 0$. Consequently, the interactions are reciprocal: all spins tend to align their phases, resulting in a synchronized state (see Fig. 2(e)) and the narrow linewidth of the emitted light [3, 27]. The population of the undriven spins, however, is not inverted and $s_{\text{ud}}^z < 0$ is obtained in the long-time limit. Therefore, the phase ϕ_{ud} of the undriven spins is repelled from the average phase $\bar{\phi}$. The phase ϕ_{d} of the driven spins remains to be attracted by the average phase $\bar{\phi}$. The competing attraction and repulsion of the phases constitute the effective nonreciprocal interactions among the atomic dipoles, summarized in Fig. 1(b).

Dynamics of the form of Eq. (4) have been previously described for a network of classical phase oscillators [15, 16]. The oscillators that tend to align with the mean field have been termed conformists. The oscillators that tend to antialign with the mean field oppose the average coherence; therefore, they have been termed contrarians. The conformist-contrarian dynamics have been connected to opinion forming, but no physical model to realize them is proposed. We have shown that the same phase interactions emerge in a superradiant laser with a fraction of undriven spins, offering a physical realization of these dynamics. In Refs. [15, 16], the nonreciprocity results in chase-and-run-away dynamics of the phases, named traveling-wave states. We now show that Eqs. (4) also result in traveling-wave states for $p_{\text{d}} < 1$, which implies emergent oscillations explaining the shift in the lasing frequency displayed in Figs. 1(a,b).

Traveling-wave states.—The mean-field equations Eqs. (3) can be solved exactly by an ansatz with constant populations $s_{\text{d,ud}}^z$, and oscillating $s_{\text{d}}^+ = |s_{\text{d}}^+| e^{i\omega t + i(\phi_{\text{d}} - \phi_{\text{ud}})}$ and $s_{\text{ud}}^+ = |s_{\text{ud}}^+| e^{i\omega t}$, where $|s_{\text{d,ud}}^+|$ is constant. We introduced the shared oscillation frequency ω , and the constant phase difference $(\phi_{\text{d}} - \phi_{\text{ud}})$ between driven and undriven spins. In the Bloch-sphere picture, the ansatz describes oscillations on circles with radii $|s_\mu^+|$ at constant s_μ^z ; see Fig. 2(d). Inserting this ansatz in Eqs. (3), the frequency of the traveling-wave states is obtained as

$$\omega = \pm \sqrt{\frac{\gamma_+}{4} \left(v - 2Vp_{\text{ud}} - \sqrt{v(v - 4Vp_{\text{ud}})} \right)}, \quad (5)$$

where $v = 2V - \gamma_+$. The frequency is shown by the

dashed line in Fig. 2(a). It matches well with the spectrum, which confirms that our ansatz of traveling-wave states explains the numerical observation of the frequency shifts in the superradiant laser. Both solutions with positive and negative frequencies are stable. The system spontaneously settles to either of the two solutions breaking parity-time symmetry [12, 18].

In active matter [9, 10], dynamical states like traveling-wave states occur via a nonreciprocal phase transition [11–13], with time-crystalline order induced by dynamical frustration [14]. Similarly, the nonreciprocal interactions between driven and undriven spins result in dynamical traveling-wave states breaking time-translation symmetry [28, 29]. This has direct physical relevance for the operation of superradiant lasers. Since the cavity output closely follows the collective spin state $a = -i(2\Omega/\kappa)S^-$, the emergent dynamics of the spins imply a frequency shift of the laser, detrimental to a stable frequency reference.

The traveling-wave states are unique to the superradiant regime of lasers. In a standard laser, where the loss rate of the cavity is small compared to the drive rate of the spins, the presence of undriven spins results in a smaller effective size of the gain medium but does not cause a frequency shift [24].

Lasing transition.—Using Eqs. (3), a stability analysis around the incoherent state [see Fig. 2(c)] yields lasing above a critical fraction of driven spins [24]

$$p_{\text{d}} > \frac{1}{2} + \frac{\gamma_+}{4V}. \quad (6)$$

Consequently, at least half of the ensemble needs to be driven for lasing to occur. If the undriven spins were absent instead of coupled to the cavity, the transition would be $p_{\text{d}} > \gamma_+/(2V)$, and lasing can be achieved for any $p_{\text{d}} > 0$ as long as V is large enough [24]. For $p_{\text{d}} = 1$, the lasing threshold reduces to $\gamma_+/V < 2$.

Spontaneous emission and dephasing.—Spontaneous emission at rate γ_- and dephasing at rate γ_z of each spin are included by adding $\sum_{\mu=\{\text{d,ud}\}} \sum_{i=1}^{N_\mu} (\gamma_- \mathcal{D}[\sigma_{\mu,i}^-] + \gamma_z \mathcal{D}[\sigma_{\mu,i}^z]/2) \rho$ to the right-hand side of the master equation (1). As a first consequence, the lasing transition of Eq. (6) changes, see [24] for the full expression. Most importantly, the incoherent drive needs to overcome the spontaneous emission to allow for population inversion. The steady-state laser power computed within the cumulant approximation for $N = 10^5$ is shown in Fig. 3(a). It exhibits a transition from small to large power compatible with the mean-field prediction (white line).

The second consequence of spontaneous emission and dephasing is that the purity of the undriven spins is no longer conserved; their coherence decays at rate $\Gamma/2 \equiv (\gamma_- + 2\gamma_z)/2$. As the undriven spins decohere, they become less important as antagonists to the driven spins. The frequency shift, which arises due to the competition

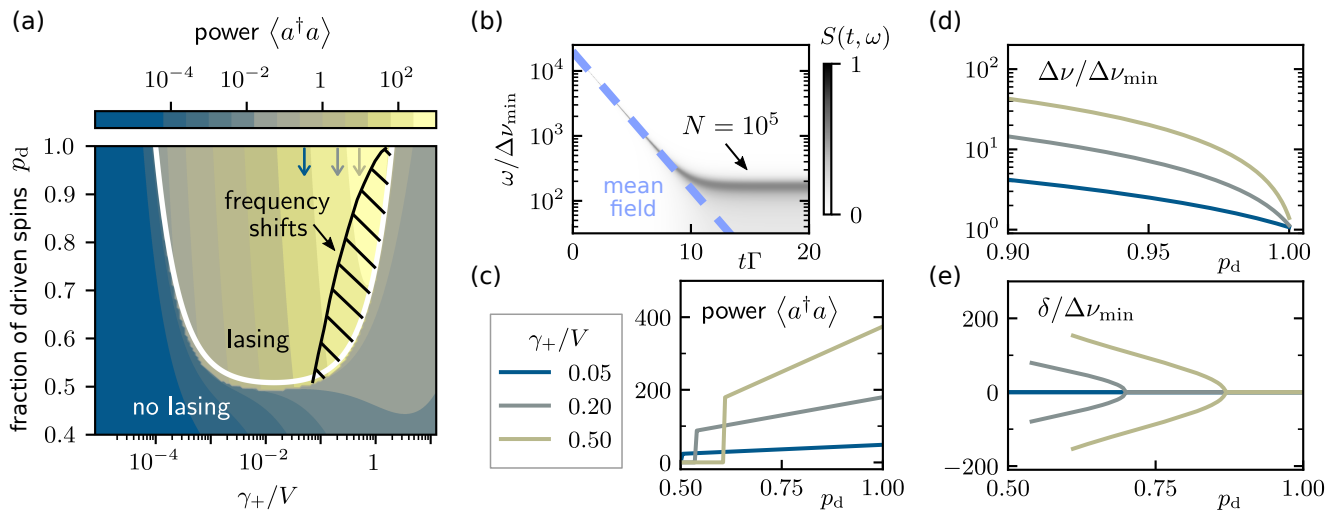


FIG. 3. Steady-state lasing properties for $N = 10^5$, and with $\gamma_-/V = 10^{-4}$ and $\gamma_z/V = 10^{-3}$ (other parameters as in Fig. 2). (a) Laser power as a function of drive rate and fraction of driven spins. The white line shows the mean-field lasing transition. The hatched region indicates the regime in which frequency shifts occur. (b) Frequency shift as a function of time for $p_d = 0.8$ and $\gamma_+ = V$. The initial state at $t = 0$ is the stationary state when $\gamma_- = \gamma_z = 0$. The dashed line is the mean-field solution, which follows an exponential decay at rate $\Gamma/2 = (\gamma_- + 2\gamma_z)/2$. The spectrum for $N = 10^5$ is shown in grayscale (arb. units). (c) Line cuts through (a) as marked by the three arrows in (a) on a linear scale. (d,e) Steady-state linewidth and frequency shifts in units of the minimum linewidth $\Delta\nu_{\min} = V/N$ (same legend as (c)).

of alignment and antialignment, consequently decreases. Figure 3(b) shows the time evolution of the frequency ω . In the mean-field limit, it exponentially decays to zero at rate Γ (dashed line). For finite N , after an initial exponential decay, a nonzero frequency shift remains in the spectrum in the long-time limit even in the presence of spontaneous emission and dephasing. This frequency shift vanishes for $N \rightarrow \infty$ consistent with the mean-field analysis [24]. The initial frequency is large compared to Γ for typical experimental parameters [3] and therefore remains observable as a transient in experiments.

Lasing properties.—To characterize the steady-state lasing, we analyze the dependence of three key properties of the laser on the fraction of driven spins p_d : the laser power, the linewidth and the frequency. The spectral properties are obtained by fitting a double-peaked Lorentzian with linewidth $\Delta\nu$ and frequency shift $\pm\delta$ to the spectrum [24]. The linewidth shown in Fig. 3(d) significantly increases as the fraction of driven spins decreases, revealing a strong spectral broadening caused by the antialignment of undriven dipoles. Taking for example $\gamma_+ = V/2$, the linewidth increases by one order of magnitude for only 3% of undriven spins. While for smaller drive rates there is less spectral broadening, the laser power is smaller, see Fig. 3(c). Finally, as shown in Fig. 3(e), a frequency shift can occur below a critical value of p_d . This regime of nonzero frequency shifts is highlighted as the hatched region in Fig. 3(a). It largely coincides with the regime of large powers where $\gamma_+ \approx V$.

Conclusion.—We have discussed a simple modification

to the model of a superradiant laser that has significant consequences. Introducing a fraction of undriven atomic spins limits the optimal operation of the laser in three ways: an increased spectral linewidth, a shift of the lasing frequency, and a reduced power. We explained these effects by identifying nonreciprocal interactions between driven and undriven atoms. While nonreciprocal interactions are known as a distinguishing feature of classical active matter, our work shows that they naturally occur in atomic quantum systems as well.

There are various directions to explore in further studies. While we have focused on a continuous incoherent drive, other proposals to achieve continuous superradiant lasing employ a beam of initially excited atoms that pass through the cavity [30–33]. If a fraction of those atoms is not excited, similar dynamics as described here may occur. Second, one can explore distributions of incoherent drive rates other than the bimodal distribution considered here. Third, the effects presented in this work will similarly occur in superradiant masers operating at microwave frequencies as they are described by the same master equation (1) [34, 35]. Having demonstrated practical implications of quantum nonreciprocal interactions will hopefully inspire future research of their applications in quantum technologies.

Acknowledgments.—We acknowledge discussions with Petr Zapletal and Marco Schiró. T.N. and C.B. acknowledge financial support from the Swiss National Science Foundation individual grant (No. 200020 200481). M.B. acknowledges funding from the European Research

Council (ERC) under the European Union's Horizon 2020 research and innovation program (Grant agreement No. 101002955 - CONQUER)

-
- [1] F. Haake, M. I. Kolobov, C. Fabre, E. Giacobino, and S. Reynaud, Superradiant laser, *Phys. Rev. Lett.* **71**, 995 (1993).
- [2] J. Chen, Active optical clock, *Chin. Sci. Bull.* **54**, 348 (2009).
- [3] D. Meiser, J. Ye, D. R. Carlson, and M. J. Holland, Prospects for a Millihertz-Linewidth Laser, *Phys. Rev. Lett.* **102**, 163601 (2009).
- [4] J. G. Bohnet, Z. Chen, J. M. Weiner, D. Meiser, M. J. Holland, and J. K. Thompson, A steady-state superradiant laser with less than one intracavity photon, *Nature* **484**, 78 (2012).
- [5] M. A. Norcia and J. K. Thompson, Cold-Strontium Laser in the Superradiant Crossover Regime, *Phys. Rev. X* **6**, 011025 (2016).
- [6] T. Laske, H. Winter, and A. Hemmerich, Pulse Delay Time Statistics in a Superradiant Laser with Calcium Atoms, *Phys. Rev. Lett.* **123**, 103601 (2019).
- [7] S. L. Kristensen, E. Bohr, J. Robinson-Tait, T. Zelevinsky, J. W. Thomsen, and J. H. Müller, Subnatural Linewidth Superradiant Lasing with Cold ^{88}Sr Atoms, *Phys. Rev. Lett.* **130**, 223402 (2023).
- [8] A. D. Ludlow, M. M. Boyd, J. Ye, E. Peik, and P. O. Schmidt, Optical atomic clocks, *Rev. Mod. Phys.* **87**, 637 (2015).
- [9] M. J. Bowick, N. Fakhri, M. C. Marchetti, and S. Ramaswamy, Symmetry, thermodynamics, and topology in active matter, *Phys. Rev. X* **12**, 010501 (2022).
- [10] S. Shankar, A. Souslov, M. J. Bowick, M. C. Marchetti, and V. Vitelli, Topological active matter, *Nat. Rev. Phys.* **4**, 380 (2022).
- [11] Z. You, A. Baskaran, and M. C. Marchetti, Nonreciprocity as a generic route to traveling states, *Proc. Natl. Acad. Sci. U.S.A.* **117**, 19767 (2020).
- [12] M. Fruchart, R. Hanai, P. B. Littlewood, and V. Vitelli, Non-reciprocal phase transitions, *Nature* **592**, 363 (2021).
- [13] F. Brauns and M. C. Marchetti, Nonreciprocal Pattern Formation of Conserved Fields, *Phys. Rev. X* **14**, 021014 (2024).
- [14] R. Hanai, Nonreciprocal frustration: Time crystalline order-by-disorder phenomenon and a spin-glass-like state, *Phys. Rev. X* **14**, 011029 (2024).
- [15] H. Hong and S. H. Strogatz, Kuramoto Model of Coupled Oscillators with Positive and Negative Coupling Parameters: An Example of Conformist and Contrarian Oscillators, *Phys. Rev. Lett.* **106**, 054102 (2011).
- [16] H. Hong and S. H. Strogatz, Conformists and contrarians in a Kuramoto model with identical natural frequencies, *Phys. Rev. E* **84**, 046202 (2011).
- [17] E. I. R. Chiacchio, A. Nunnenkamp, and M. Brunelli, Nonreciprocal Dicke model, *Phys. Rev. Lett.* **131**, 113602 (2023).
- [18] T. Nadolny, C. Bruder, and M. Brunelli, Nonreciprocal synchronization of active quantum spins, *Phys. Rev. X* **15**, 011010 (2025).
- [19] R. Hanai, D. Ootsuki, and R. Tazai, Photoinduced non-reciprocal magnetism (2024), arXiv:2406.05957.
- [20] R. Kubo, Generalized cumulant expansion method, *Journal of the Physical Society of Japan* **17**, 1100 (1962).
- [21] H.-P. Breuer and F. Petruccione, *The Theory of Open Quantum Systems* (Oxford University Press, 2007).
- [22] M. Xu, D. A. Tieri, E. C. Fine, J. K. Thompson, and M. J. Holland, Synchronization of two ensembles of atoms, *Phys. Rev. Lett.* **113**, 154101 (2014).
- [23] D. Plankensteiner, C. Hotter, and H. Ritsch, Quantum-Cumulants.jl: A Julia framework for generalized mean-field equations in open quantum systems, *Quantum* **6**, 617 (2022).
- [24] See Supplemental Material, for details on cumulant expansion, spectrum calculation, comparison to standard lasers, stability analysis, and Lorentzian fits.
- [25] H. Spohn, Kinetic equations from Hamiltonian dynamics: Markovian limits, *Rev. Mod. Phys.* **52**, 569 (1980).
- [26] The thermodynamic limit $N \rightarrow \infty$ is well defined, when simultaneously decreasing $\Omega \rightarrow 0$, such that $V \propto N\Omega^2 = \text{constant}$.
- [27] B. Zhu, J. Schachenmayer, M. Xu, F. Herrera, J. G. Restrepo, M. J. Holland, and A. M. Rey, Synchronization of interacting quantum dipoles, *New Journal of Physics* **17**, 083063 (2015).
- [28] K. Sacha and J. Zakrzewski, Time crystals: a review, *Rep. Prog. Phys.* **81**, 016401 (2017).
- [29] P. Kongkhambut, J. Skulte, L. Mathey, J. G. Cosme, A. Hemmerich, and H. Keßler, Observation of a continuous time crystal, *Science* **377**, 670 (2022).
- [30] G. A. Kazakov and T. Schumm, Active optical frequency standards using cold atoms: Perspectives and challenges, in *2014 European Frequency and Time Forum (EFTF)* (2014) pp. 411–414.
- [31] H. Liu, S. B. Jäger, X. Yu, S. Touzard, A. Shankar, M. J. Holland, and T. L. Nicholson, Rugged mHz-Linewidth Superradiant Laser Driven by a Hot Atomic Beam, *Phys. Rev. Lett.* **125**, 253602 (2020).
- [32] M. Tang, S. A. Schäffer, and J. H. Müller, Prospects of a superradiant laser based on a thermal or guided beam of ^{88}Sr , *Phys. Rev. A* **106**, 063704 (2022).
- [33] F. Famà, S. Zhou, B. Heizenreder, M. Tang, S. Bennetts, S. B. Jäger, S. A. Schäffer, and F. Schreck, Continuous cavity QED with an atomic beam, *Phys. Rev. A* **110**, 063721 (2024).
- [34] D. M. Arroo, N. M. Alford, and J. D. Breeze, Perspective on room-temperature solid-state masers, *Appl. Phys. Lett.* **119**, 140502 (2021).
- [35] Q. Wu, Y. Zhang, X. Yang, S.-L. Su, C. Shan, and K. Mølmer, A superradiant maser with nitrogen-vacancy center spins, *Sci. China Phys. Mech. Astron.* **65**, 1 (2022).

Supplemental material for “Nonreciprocal interactions induce frequency shifts in superradiant lasers”

1. Cumulant expansion

To calculate the output power and the spectrum for large but finite N , we use a cumulant expansion [20] neglecting third and higher-order correlations. Additionally, we exploit the permutational invariance of driven and undriven spins respectively, and the global $U(1)$ -symmetry to set terms like $\langle a \rangle$ or $\langle a^\dagger \sigma_\mu^+ \rangle$ equal to zero. This leads to a closed set of eight equations,

$$\begin{aligned}
\frac{d}{dt} s_d^z &= -\gamma_-(s_d^z + 1) - \gamma_+(s_d^z - 1) - 4\Omega \text{Im}[\langle a^\dagger \sigma_d^- \rangle], \\
\frac{d}{dt} s_{ud}^z &= -\gamma_-(s_{ud}^z + 1) - 4\Omega \text{Im}[\langle a^\dagger \sigma_{ud}^- \rangle], \\
\frac{d}{dt} \langle a^\dagger a \rangle &= -\kappa \langle a^\dagger a \rangle + 2\Omega (N_d \text{Im}[\langle a^\dagger \sigma_d^- \rangle] + N_{ud} \text{Im}[\langle a^\dagger \sigma_{ud}^- \rangle]) \\
\frac{d}{dt} \langle a^\dagger \sigma_d^- \rangle &= -(\gamma_+ + \Gamma + \kappa) \langle a^\dagger \sigma_d^- \rangle / 2 + i\Omega \left((N_d - 1) \langle \sigma_d^+ \sigma_d^- \rangle + \frac{1 + s_d^z}{2} + N_{ud} \langle \sigma_{ud}^+ \sigma_d^- \rangle + \langle a^\dagger a \rangle s_d^z \right) \\
\frac{d}{dt} \langle a^\dagger \sigma_{ud}^- \rangle &= -(\Gamma + \kappa) \langle a^\dagger \sigma_{ud}^- \rangle / 2 + i\Omega \left((N_{ud} - 1) \langle \sigma_{ud}^+ \sigma_{ud}^- \rangle + \frac{1 + s_{ud}^z}{2} + N_d \langle \sigma_d^+ \sigma_{ud}^- \rangle + \langle a^\dagger a \rangle s_{ud}^z \right), \\
\frac{d}{dt} \langle \sigma_d^+ \sigma_d^- \rangle &= -(\gamma_+ + \Gamma) \langle \sigma_d^+ \sigma_d^- \rangle + 2\Omega s_d^z \text{Im}[\langle a^\dagger \sigma_d^- \rangle], \\
\frac{d}{dt} \langle \sigma_{ud}^+ \sigma_{ud}^- \rangle &= -\Gamma \langle \sigma_{ud}^+ \sigma_{ud}^- \rangle + 2\Omega s_{ud}^z \text{Im}[\langle a^\dagger \sigma_{ud}^- \rangle] \\
\frac{d}{dt} \langle \sigma_d^+ \sigma_{ud}^- \rangle &= -(\gamma_+ / 2 + \Gamma) \langle \sigma_d^+ \sigma_{ud}^- \rangle + i\Omega \left(s_{ud}^z \langle a^\dagger \sigma_d^- \rangle^* - s_d^z \langle a^\dagger \sigma_{ud}^- \rangle \right).
\end{aligned}$$

We use the Julia package QuantumCumulants.jl [23] to integrate these equations numerically.

2. Spectrum

The spectrum is computed within the cumulant expansion approximation using the quantum regression theorem [21]. By factorizing $\langle \sigma_\mu^z(t + \tau) a^\dagger(t + \tau) a(t) \rangle \approx s_\mu^z(t + \tau) \langle a^\dagger(t + \tau) a(t) \rangle$, the two-time correlations evolve according to

$$\frac{d}{d\tau} \mathbf{c}(t, \tau) = M(t + \tau) \mathbf{c}(t, \tau), \quad \mathbf{c}(t, \tau) = \begin{pmatrix} \langle a^\dagger(t + \tau) a(t) \rangle \\ \langle \sigma_d^+(t + \tau) a(t) \rangle \\ \langle \sigma_{ud}^+(t + \tau) a(t) \rangle \end{pmatrix}, \quad M(t + \tau) = \begin{pmatrix} -\kappa/2 & iN_d\Omega & iN_{ud}\Omega \\ -i\Omega s_d^z(t + \tau) & -(\Gamma + \gamma_+)/2 & 0 \\ -i\Omega s_{ud}^z(t + \tau) & 0 & -\Gamma/2 \end{pmatrix}. \quad (\text{S1})$$

In the steady state $t \rightarrow \infty$, where s_μ^z obtains a constant value, the matrix M is time independent, and the steady-state spectrum can be calculated using the Laplace transform,

$$S(\omega) = \lim_{t \rightarrow \infty} \int_{-\infty}^{\infty} d\tau \langle a^\dagger(t + \tau) a(t) \rangle e^{i\omega\tau} = 2 \text{Re} \{ [(i\omega - M)^{-1} \mathbf{c}_{ss}]_1 \}. \quad (\text{S2})$$

Here, the subscript 1 refers to the first component of the vector, and $\mathbf{c}_{ss} = \lim_{t \rightarrow \infty} \mathbf{c}(t, 0)$.

The spectrum in Fig. 3(b) can be calculated by a discrete Fourier transform of solutions of Eq. (S1) in consecutive time intervals. By using that s_μ^z changes at rate Γ during the transient, which is small compared to the typical frequency ω , we set $s_\mu^z(t + \tau) = s_\mu^z(t)$ constant for each time interval and use the Laplace transform at each time t to approximately calculate the spectrum,

$$S(t, \omega) = \int_{-\infty}^{\infty} d\tau \langle a^\dagger(t + \tau) a(t) \rangle e^{i\omega\tau} \approx 2 \text{Re} \{ [(i\omega - M(t))^{-1} \mathbf{c}(t, 0)]_1 \}. \quad (\text{S3})$$

3. Comparison to standard laser

The mean-field equations of the master equation Eq. (1) in the presence of the cavity field $\alpha = \langle a \rangle$ are

$$\begin{aligned}
\frac{d}{dt} s_d^z &= -\gamma_-(s_d^z + 1) - \gamma_+(s_d^z - 1) + 4\Omega \text{Im}[\alpha s_d^+], \\
\frac{d}{dt} s_{ud}^z &= -\gamma_-(s_{ud}^z + 1) + 4\Omega \text{Im}[\alpha s_{ud}^+], \\
\frac{d}{dt} s_d^+ &= -(\gamma_+ + \gamma_- + 2\gamma_z) s_d^+ / 2 - i\Omega \alpha^* s_d^z, \\
\frac{d}{dt} s_{ud}^+ &= -(\gamma_- + 2\gamma_z) s_{ud}^+ / 2 - i\Omega \alpha^* s_{ud}^z, \\
\frac{d}{dt} \alpha &= -\kappa \alpha / 2 - iN\Omega s^-.
\end{aligned} \tag{S4}$$

They result in Eqs. (3) after the adiabatic elimination of the cavity field, $\alpha \rightarrow -2iN\Omega s^- / \kappa$.

In a standard laser, the cavity is a ‘good’ cavity with a decay rate κ that is small compared to the incoherent gain and damping of the atoms. In this case, one can adiabatically eliminate the spin degrees of freedom in Eq. (S4) by setting $\dot{s}_\mu^z = \dot{s}_\mu^+ = 0$ to obtain

$$\frac{d}{dt} \alpha = \alpha \left(-\frac{\kappa}{2} + 2Np_d \frac{\gamma_+ - \gamma_-}{\tilde{\Gamma}_d^2 / \Omega^2 + 8|\alpha|^2} - 2Np_{ud} \frac{\gamma_-}{\tilde{\Gamma}_{ud}^2 / \Omega^2 + 8|\alpha|^2} \right), \tag{S5}$$

where we have defined $\tilde{\Gamma}_d^2 = (\gamma_- + \gamma_+)(\gamma_- + \gamma_+ + 2\gamma_z)$ and $\tilde{\Gamma}_{ud}^2 = \gamma_-(\gamma_- + 2\gamma_z)$. Since the term in brackets on the right-hand side is real-valued, there are no oscillations and no traveling-wave states. The lasing transition (obtained by expanding around $\alpha = 0$) is

$$p_d \frac{\gamma_+ - \gamma_-}{\tilde{\Gamma}_d^2} - p_{ud} \frac{\gamma_-}{\tilde{\Gamma}_{ud}^2} > \frac{\kappa}{4N\Omega^2} = \frac{1}{2V}. \tag{S6}$$

For any nonzero p_d , the drive rate γ_+ can be increased sufficiently to obtain lasing. This contrasts the behavior of the superradiant laser, where no lasing can be obtained for $p_d < 1/2$, see Eq. (6) or Eq. (S8).

4. Mean-field stability analysis

The mean-field equations including decay at rate γ_- and dephasing at rate $\Gamma = \gamma_- + 2\gamma_z$ are

$$\begin{aligned}
\frac{d}{dt} s_d^+ &= V s^+ s_d^z - (\Gamma + \gamma_+) s_d^+ / 2, \\
\frac{d}{dt} s_{ud}^+ &= V s^+ s_{ud}^z - \Gamma s_{ud}^+ / 2, \\
\frac{d}{dt} s_d^z &= -4V \text{Re}[s_d^- s^+] - \gamma_-(1 + s_d^z) + \gamma_+(1 - s_d^z), \\
\frac{d}{dt} s_{ud}^z &= -4V \text{Re}[s_{ud}^- s^+] - \gamma_-(1 + s_{ud}^z),
\end{aligned} \tag{S7}$$

where again $s^+ = p_d s_d^+ + p_{ud} s_{ud}^+$. The fixed point, which characterizes the incoherent state, is $s_{d,ud}^+ = 0$, $s_d^z = (\gamma_+ - \gamma_-) / (\gamma_+ + \gamma_-)$, and $s_{ud}^z = -1$. From a stability analysis around this fixed point, we obtain the lasing transition as

$$p_d > \frac{1}{2} \left(1 + \frac{\gamma_-}{\gamma_+} \right) \left(1 + \frac{\Gamma}{V} + \frac{\gamma_+}{2V} \right), \tag{S8}$$

which reduces to Eq. (6) when $\gamma_- = \gamma_z = 0$, and defines the white line shown in Fig. 3(a).

If the undriven spins do not couple to the cavity (setting $V = 0$ in the second and fourth line of Eqs. (S7)), the critical coupling is

$$p_d > \frac{(\gamma_- + \gamma_+)(\Gamma + \gamma_+)}{2(\gamma_+ - \gamma_-)V} \xrightarrow{\gamma_- = \Gamma = 0} \frac{\gamma_+}{2V}. \tag{S9}$$

The lasing threshold is smaller in this case compared to the threshold set by Eq. (S8). Therefore, the undriven spins increase the lasing threshold more when they are coupled to the cavity compared to when they are not coupled.

5. Lorentzian fits

To obtain the linewidth and the frequency shift in Figs. 3(d,e), we fit the sum of two Lorentzian distributions,

$$\frac{A}{\pi} \left(\frac{\Delta\nu}{\Delta\nu^2 + (\omega - \delta)^2} + \frac{\Delta\nu}{\Delta\nu^2 + (\omega + \delta)^2} \right), \quad (\text{S10})$$

with amplitude A and linewidth $\Delta\nu$, displaced by $\pm\delta$, to the spectrum. The fitted linewidth and frequency shift agree well with the real and imaginary parts of the eigenvalues of matrix M of Eq. (S1).

6. Dependence of frequency shift on system size

Figure S1 shows the time evolution of the frequency shift for different values of N . For $N \rightarrow \infty$, the spectrum approaches the mean-field prediction (dashed line). The cumulant expansion thus predicts that the frequency shift vanishes for $t \rightarrow \infty$ in the thermodynamic limit consistent with the mean-field analysis.

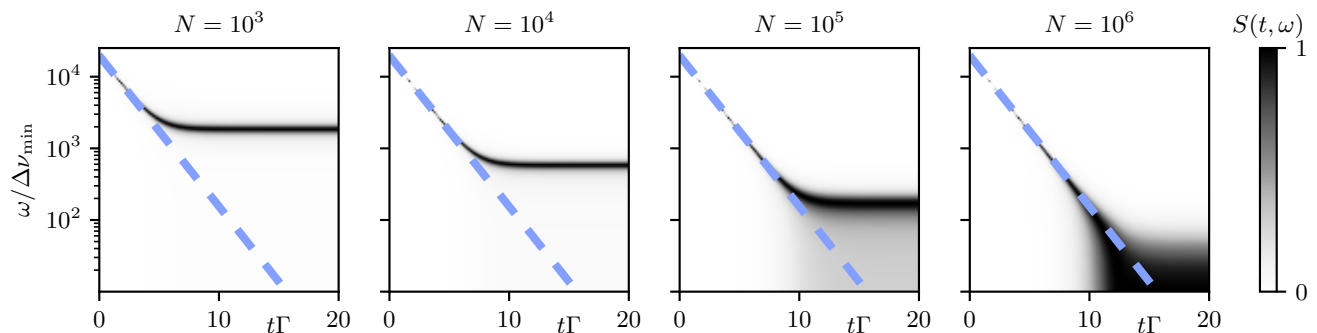


FIG. S1. Time dependence of the frequency shift in the spectrum for different values of N . The spectrum is normalized to a maximum value of 1 for each time t . The dashed line is the mean-field prediction of the frequency. Parameters as in Fig. 3 with N specified for each panel.